Coseismic slip and afterslip of the 2024 Hyuganada earthquake modulated by subducted seamount

Yuji Itoh[1]

[1]Earthquake Research Institute, The University of Tokyo, Tokyo, Japan

Key Points:

- The 2024 Hyuganada earthquake occurred at the leading edge of a seamount in the creeping megathrust due to ridge subduction
- The subducted seamount probably impeded up-dip mainshock rupture propagation and slowed up-dip afterslip migration speed
- An along-strike segment of the mainshock was left unruptured during the afterslip, but whether it causes the next earthquake remains elusive

Corresponding author: Yuji Itoh, `yitoh@eri.u-tokyo.ac.jp`

Abstract

Subducted rough topography complicates seismic and aseismic slip behavior. The 2024 M 7.1 Hyuganada earthquake occurred along the megathrust with ridge subduction. We inferred coseismic slip and afterslip using geodetic displacements to observationally illustrate the role of subducted seamounts in modulating seismic and aseismic slip processes. The inferred mainshock was confined in the down-dip of the seamount, suggesting that the seamount impeded the mainshock rupture initiated under enhanced compression. The inferred afterslip peaked at the up-dip of the mainshock peak with four aftershock clusters. Various onset timings of these clusters suggest the afterslip front migration slowed down when passing through the seamount. An along-strike neighbor segment of the mainshock peak was left unruptured during the afterslip, but whether this segment causes another earthquake remains elusive only with the available observations. Our results geodetically highlight the mechanical heterogeneity of megathrust with ridge subduction at an order of 10 km.

Plain Language Summary

The 2024 Hyuganada earthquake occurred offshore Kyushu, Japan, where the oceanic Philippine Sea Plate subducts beneath the continental Amur plate with the highly variable seafloor topography called Kyushu-Palau ridge. Simulations have shown that the subduction of irregular topography yields complex fault slip behavior on and around it, so we observationally imaged fault slip processes during and after the 2024 earthquake to illustrate the role of seamounts in impacting slip behavior on the natural fault. Our analysis suggested that (1) the mainshock was impeded when its slip front entered the seamount zone and (2) the post-mainshock aseismic afterslip front migrated more slowly when passing the seamount zone. We also did not identify a significant amount of slip in an along-strike neighbor segment of the mainshock slip area during the afterslip. The question of whether this segment causes the next earthquake remains, however, elusive because only limited geophysical observations are available.

1 Introduction

In Hyuganada, southwestern Japan, the Philippine Sea Plate subducts beneath the Amur plate. In contrast with off-Shikoku where few megathrust earthquakes except the great Nankai earthquake sequences have occurred (e.g., Ando, 1975; Sagiya & Thatcher, 1999), many earthquakes up to M 7.5 have frequently occurred along their interface offshore Hyuganada (Figure 1)(e.g., Yagi et al., 1998, 1999). However, further larger earthquakes (i.e., M > 7.5) have occurred much less frequently than expected from the convergence rate there (Ioki et al., 2023; K. Wang & Bilek, 2014). The most recent notable quake is the 2024 M_{JMA} 7.1 Hyuganada earthquake on August 8, 2024, which occurred near the rupture areas of the two 1996 Hyuganada earthquakes (M_w 6.8 and 6.7 for the October and the December events, respectively; Yagi et al., 1999)(Figure 1). Such a regional characteristic of seismogenesis has been understood as a result of the subduction of rough seafloor such as seamounts (e.g., K. Wang & Bilek, 2014). The subduction of Kyushu-Palau Ridge (KPR) on the incoming Philippine Sea supports this interpretation (e.g., Arai et al., 2023; Yamamoto et al., 2013)(Figure 1a). Low margin-normal contraction and resultant low slip deficit rates during the interseismic stage (T. Nishimura et al., 2018; S. Nishimura & Hashimoto, 2006; Noda et al., 2018; Okazaki et al., 2021; Sagiya et al., 2000; Sagiya, 2004; Wallace et al., 2009) support the steady creep nature of rugged plate interface due to the seamount/ridge subduction (e.g., Perfettini et al., 2010; K. Wang & Bilek, 2011, 2014).

Subducted seamounts locally modify stress distribution and thus complicate fault slip and locking behavior throughout the earthquake cycle. For example, the plate interface fault on top of the subducted seamount favors creep due to the heterogeneous

stress distribution (K. Wang & Bilek, 2011). They sometimes also host afterslip (e.g., Itoh et al., 2023; Perfettini et al., 2010). In contrast, compressional stress and drainage along the megathrust are enhanced at the leading flank of subducted seamounts, which provides a favorable condition for ordinary earthquake generations (Ruh et al., 2016; Sun et al., 2020). Creeping subducted seamounts may impede earthquake rupture approaching them as a soft barrier (K. Wang & Bilek, 2011). Such a contrast in slip modes on and around subducted seamounts clearly explains the spatial separation of ordinary and slow earthquake activities on and around a subducted seamount offshore Ibaraki, northeastern Japan (Kubo & Nishikawa, 2020; Mochizuki et al., 2008). The 2024 mainshock epicenter and the two 1996 events are located within the subducted KPR inferred from a low seismic velocity layer near the plate interface (Yamamoto et al., 2013). Within this wide zone having possible geometrical irregularities, a local seaount, inferred from local high reduced-to-pole (RTP) magnetic anomaly (Arai et al., 2023; Okino, 2015), is located at the up-dip extension of the two 1996 rupture areas and the 2024 epicenter (Figure 1a). Therefore, the 2024 event and its afterslip give us a valuable opportunity to investigate the mechanical link between seismic/aseismic fault slip and the subducted KPR, particularly, the up-dip seamount. Hence, in this study, we derive coseismic slip and 1-week afterslip of the 2024 Hyuganada earthquake using Global Navigation Satellite System (GNSS) data to image the interlaced seismic and aseismic slip patches. Then, by comparing them with aftershocks, ordinary and slow earthquakes, and the subducted seamount location, we observationally illustrate the role of seamounts in modulating seismic and aseismic slip behavior.

2 Data analysis and slip inversion

2.1 GNSS data analysis

We employed GNSS coordinate time series processed by the Nevada Geodetic Laboratory (Blewitt et al., 2018) to derive co- and post-seismic displacements associated with the 2024 Hyuganada earthquake. First, we estimated coseismic displacements using time series at an interval of 5 minutes to minimize postseismic deformation contaminated in the coseismic displacement (Figure 2b, d, and f). We skipped removal of multipath (Choi et al., 2004; Itoh & Aoki, 2022; Ragheb et al., 2007) and common mode errors (Wdowinski et al., 1997) because we are interested in only an instantaneous displacement step. Next, we estimated coseismic and postseismic displacements simultaneously from daily coordinates by fitting a function (Equation (1))

$$x(t) = a + \left(b + c\log\left(1 + \frac{t}{\tau} \right) \right) \mathrm{H}(t) \tag{1}$$

where, $x(t)$ is a position at time t with $t = 0$ the mainshock date, $\mathrm{H}(t)$ is a Heaviside function, and τ is a time constant (Figure 2a, c, and e). We determined a, b, and c by linear least square regression and τ by grid search. Here, we used the data ranging from one month before to one week after the mainshock date. We let each component at each site have a different τ because this trajectory model fit aims to extract co- and post-seismic displacements from fluctuating time series. Therefore, we do not interpret the obtained τ values themselves. Then, we separated the postseismic displacement by subtracting the coseismic displacement derived from the 5-minute coordinates from the model prediction from Equation (1). We estimated the errors for the coseismic displacements by combining the standard deviation of the pre- and post-mainshock position estimation. For the postseismic displacement errors, we combined the standard deviation of residual daily time series and the coseismic displacement errors.

For the following reasons, we combined the daily and 5-minute coordinates to derive co- and post-seismic displacements. Typical analysis routine of daily coordinates uses all the observables from each day, meaning that the mainshock day position is derived from observables both before and after the mainshock; therefore, the mainshock day co-

ordinate is inevitably biased. This compels us to set the origin of postseismic deformation to the next day of the mainshock occurrence which usually significantly underestimates the post-seismic displacement estimates (Twardzik et al., 2019). In our case, our coseismic displacements derived from the 5-min coordinates do not match with those measured using the daily coordinate on the mainshock day or the next day (Figure 2). Measuring postseismic displacements from the next day would decrease the postseismic displacement estimate by 25% at G088 for the east component (Figures 2a-b), which would impact the resultant afterslip amount.

2.2 Slip inversion

We inverted the obtained coseismic and postseismic displacements to infer coseismic slip and 1-week afterslip, respectively (Figure 3), using an inversion code SDM (L. Wang et al., 2009; R. Wang et al., 2013a). We discretized the three-dimensional curved slab interface (Iwasaki et al., 2015) into small rectangle subfaults and computed Green's functions in an isotropic homogeneous half-space (Okada, 1985). To stabilize the solution, we imposed a smoothness constraint on the slip. Also, the rake angle was constrained to be between 30 and 150 degrees. For our preferred afterslip solution, we forced the afterslip on subfaults with ≥ 2 m coseismic slip to be zero to assure that the substantial part of coseismic slip and afterslip do not overlap with each other (e.g., Itoh et al., 2019; Miyazaki et al., 2004; Scholz, 1998). We used the horizontal and vertical displacements for the coseismic slip inversion whereas we used only the horizontal displacements for the afterslip inversion because the postseismic vertical displacements did not exhibit a systematic pattern (Figures 3a-b and S1). We chose a strength of the smoothness constraint based on a trade-off curve between misfits and slip roughness (Figures S2 and S3). All the data were weighted according to the observation error of the displacements.

3 Results and discussion

3.1 Coseismic slip and afterslip

The estimated coseismic slip is located next to the rupture areas of the two 1996 earthquakes (Figure 3a). The primary peak of the afterslip is located up-dip of the mainshock rupture area (Figure 3b), contrary to the down-dip afterslips following the two 1996 earthquakes (Figure 1a; Yagi et al., 2001). Without the mask of slip in the afterslip estimation, the substantial part of the afterslip overlaps with the coseismic slip area (Figure S4a). Such overlap is unlikely in terms of elementary behavior of frictional fault (e.g., Scholz, 1998) and most of the past observations (e.g., Itoh et al., 2019; Miyazaki et al., 2004; Perfettini et al., 2010; Yagi et al., 2001). Furthermore, both models yielded similar surface displacement fit (Figures 3b and S4a). For these reasons, we found it more reasonable to choose the model with the mask. We noticed another afterslip patch to the southwest away from the mainshock slip and a unruptured segment between this separated afterslip patch and the mainshock peak (Figure 3b). To verify this patch and the unruptured segment, we carried out two more test inversions in which the southwestern or the entire down-dip part of the model domain are masked in addition to the coseismic slip peak area (Figures S4b-c). We gained a slip peak just up-dip of the masked zone in this southwest area when we masked the entire down-dip subfaults (Figures S4c). When we only masked the southwestern corner of the model domain, the down-dip afterslip peak is shifted toward the along-strike neighbor segment to the masked area (Figures S4b). Although all the test afterslip models produced similar fitting performance to the preferred model, these tests demonstrate that the down-dip afterslip is needed to explain the observation and this down-dip afterslip possibly extends to the southwest away from the mainshock rupture area as seen in the preferred model. Also, in all the tests, afterslip was not inferred in the along-strike neighbor segment south of the mainshock rupture area. Hence, we concluded that the distant afterslip patch to the southwest and the

unruptured mainshock neighbor segment are not artifacts. The inferred moment magnitude of the preferred coseismic slip and afterslip models is M_w 7.0, and M_w 6.7, respectively, with a rigidity of 30 GPa.

3.2 Possible modulation of slip processes by the subducted seamount

The estimated coseismic slip and afterslip are located within the broad estimate of the subducted KPR by Yamamoto et al. (2013). Inside this broad zone, the RTP magnetic anomaly suggests heterogeneous megathrust topography, and the estimated coseismic slip is located on the down-dip extension of a local seamount (Figure 3a) (Arai et al., 2023; Okino, 2015). We speculate that the coseismic slip was impeded by the seamount acting as a soft barrier (K. Wang & Bilek, 2011), similar to an example of the 2008 Ibaraki-oki earthquake in the Japan Trench subduction zone (Kubo & Nishikawa, 2020). The occurrence of this mainshock in the low slip deficit rate area (Igarashi, 2020; T. Nishimura et al., 2018; S. Nishimura & Hashimoto, 2006; Noda et al., 2018; Wallace et al., 2009; Yamashita et al., 2012) might pose a question to its occurrence mechanism considering the classical framework of backslip model (Savage, 1983). We speculate that there exists an unresolved local highly locked area in the mainshock zone and its rupture occurrence was assisted by the down-dip compression enhanced by the up-dip seamount (Sun et al., 2020).

The complementary afterslip has a primary peak at the up-dip extension of the mainshock accompanied by the aftershock activity (Figures 3b and 4a). This 1-week aftershock activity provides another interesting insight into the afterslip processes up-dip of the mainshock rupture (Figure 4a). In the subsequent discussion, we assume that the aftershock migration front marks the migration front of afterslip (e.g., Kato & Obara, 2014; Peng & Zhao, 2009; Perfettini & Avouac, 2004; Perfettini et al., 2018). We do not perform time-dependent afterslip inversions because the dominant migration process finished around one day following the mainshock (Figure 4b-d) and the 5-minute GNSS coordinates would be too noisy to resolve temporal evolution of slip offshore considering the anticipated signal to noise ratio (Figure 2) (e.g., Itoh & Aoki, 2022; Twardzik et al., 2019). The one-dimensional aftershock front migration in the longitudinal and the latitudinal direction is well characterized as a logarithmic expansion with time as observed in many other cases (e.g., Frank et al., 2017; Kato & Obara, 2014; Peng & Zhao, 2009; Ross et al., 2017) (Figures 4b-c), so does the afterslip front. Among these 1-week aftershocks, we visually identified four clusters of them, from AF1 to AF4 (Figure 4a). AF1 and AF2 are located next to the coseismic slip peak while AF3 and AF4 are located further up-dip, near the up-dip edge of the 1-week cumulative afterslip patch. In the epicentral distance versus logarithmic time plot, the activation of AF1, AF2, and AF4 mostly falls on the same envelope curve of the seismicity migration front (Figures 4d) as expected from the one-dimensional migration behavior. However, the activation timing of cluster AF3 is similar to cluster AF4 although the epicentral distance of AF3 is $\sim$ 20 km shorter than AF4. This means that the activation of AF3 is significantly delayed. Only cluster AF3 is located up-dip of the seamount, so we propose that the seamount impacted the up-dip migration speed of afterslip from AF1 and AF2 to AF3. Numerical simulations of afterslip demonstrate that afterslip migration speed is slower when effective normal stress on the interface is higher (Ariyoshi et al., 2019). As subducted seamounts produce higher effective normal stress from its top to the down-dip leading flank (Ruh et al., 2016; Sun et al., 2020), the effective normal stress along the migration path between A1/A2 and A3 could be higher than that between AF2 and AF4, which is probably responsible for the delay of afterslip front and aftershock migration. We cannot rule out the possibility that AF3 was activated by different processes such as a down-dip migration of shallow slip earthquakes which happened in 2010 (Uchida et al., 2020). Yet, we conclude that the possible contrast in afterslip migration observationally unveiled another hidden role of seamounts in modulating fault slip behavior.

This up-dip afterslip patch extends to the narrow area among the two 1996 and the 2024 mainshock rupture areas (Figure 3b), marked by the presence of clustered aftershocks AF1 (Figure 4a). These interlaced seismic and aseismic peaks illustrate the presence of mechanical heterogeneity at a 10 km scale, which is usually challenging to resolve for offshore megathrust. The presence of this upcoming afterslip area might have impeded the 2024 earthquake rupture (e.g., Itoh et al., 2023; Rolandone et al., 2018) and prevented it from entering the 1996 rupture areas. The southwesternmost afterslip patch away from the mainshock rupture was perhaps triggered by dynamic stress perturbation (Figure 3b), similar to some earlier examples (e.g., Itoh et al., 2023; Rolandone et al., 2018; Wallace et al., 2018).

3.3 Unruptured segment next to the mainshock area

The 1-week afterslip is lacking in the segment south of the mainshock rupture, where only a few aftershocks occurred during the first week (Figure 3b). These observations question whether this gap will cause another large earthquake in the future loaded by the 2024 coseismic slip and subsequent afterslip. This is an important question in terms of disaster mitigation, so here we discuss whether this segment could host large seismic rupture. The low interseismic slip deficit rate in this segment could indicate that it would not cause large earthquakes. It also implies that the 2024 mainshock rupture was arrested by this creeping zone acting as a soft barrier (e.g., Nishikawa et al., 2019; Rolandone et al., 2018; Scholz, 1998; K. Wang & Bilek, 2011). Yet, other observational features do not agree with such a creeping soft barrier scenario for this unruptured segment. First, the activity of various seismic and aseismic activities in this gap, such as ordinary earthquakes (JMA hypocenters and Takemura et al., 2020b), repeating earthquakes (Igarashi, 2020; Yamashita et al., 2012), and short- and long-term slow slip events (Okada et al., 2022; Ozawa et al., 2024; Takagi et al., 2016, 2019), seems lower than in the surrounding (Figures 3c-d). This observational feature favors rather the presence of a very local locked patch there, which is, however, geodetically unresolved. Also, if this unruptured segment has velocity-strengthening friction to steadily creep, the observed absence of a significant amount of afterslip is peculiar unless a very large contrast in frictional parameters exists around the mainshock peak (Marone et al., 1991; Perfettini & Avouac, 2004; Scholz, 1998). Thus, the actual locking state of this segment remains elusive only with the available observations and so does the possibility of future large ruptures there. Continuous efforts in careful monitoring of seismic and aseismic activities in the region might provide us with new clues. Either way, the lines of interpretation of these observations suggest the presence of short-wavelength heterogeneity of frictional parameters and stress state on the megathrust inside the subducted KPR (Yamamoto et al., 2013).

4 Summary

The 2024 Hyuganada earthquake occurred along the creeping megathrust due to the presence of subducted KPR. We inferred the coseismic slip and 1-week afterslip of the 2024 Hyuganada earthquake using the observed displacements by GNSS. The comparison of the inferred slip models with the aftershocks, the ordinary earthquakes before the mainshocks, the slow earthquakes, and the local seamount, we illustrated the role of subducted seamounts in controlling coseismic and afterslip behavior (Figure 5). The mainshock occurred in the down-dip extension of the subducted seamount. As subducted seamounts enhance the compressional stress in its leading flank, developing favorable conditions for ordinary earthquake generation, the mainshock occurrence in the low interseismic slip deficit megathrust was probably assisted by the up-dip seamount (Figure 5a). During the coseismic stage (Figure 5b), the mainshock rupture likely extended toward the up-dip direction, which was arrested by the subducted seamount acting as a soft barrier. The northward rupture expansion was probably arrested by the megathrust which hosted the subsequent afterslip. Following the mainshock (Figure 5c), we iden-

tified a few patches of the 1-week afterslip. The primary patch is located up-dip of the mainshock peak, which is accompanied by the four aftershock clusters. Based on the spatiotemporal aftershock activity, we proposed that the up-dip expansion of the afterslip front is slowed down while passing the seamount. With the series of afterslip inversion tests, we confirmed that a segment south of the mainshock was hardly involved in the afterslip, consistent with the scarce aftershock activity during the first week. We concluded that whether this segment is interseismically locked and causes the next earthquake remains elusive after examining the available geophysical observations.

Open Research Section

The GNSS coordinates (Blewitt et al., 2018) are available as Nevada Geodetic Laboratory (2024). The plate model (Iwasaki et al., 2015) is available as Iwasaki (2024). Tectonic tremors (Yamashita et al., 2015, 2021) and repeaters (Igarashi, 2020) are available at Kano et al. (2018); Science of Slow Earthquakes (2024). The slip model of Yagi et al. (1998) is available at Earthquake Source Model Database (2024) in SRCMOD (Mai & Thingbaijam, 2014). The CMT solutions of Takemura et al. (2020b) are available at Takemura et al. (2020a). The JMA hypocenter catalog are available at Japan Meteorological Agency (2024a, 2024b). The slip inversion code SDM (L. Wang et al., 2009; R. Wang et al., 2013a) is available as R. Wang et al. (2013b). We will upload our products to Zenodo once the manuscript is accepted for publication. We provide their files in a zip file attached in the submission for peer review.

References

Ando, M. (1975). Source mechanisms and tectonic significance of historical earthquakes along the nankai trough, japan. *Tectonophysics*, *27*(2), 119-140. Retrieved from https://www.sciencedirect.com/science/article/pii/004019517590102X doi: https://doi.org/10.1016/0040-1951(75)90102-X

Arai, R., Miura, S., Nakamura, Y., Fujie, G., Kodaira, S., Kaiho, Y., ... others (2023). Upper-plate conduits linked to plate boundary that hosts slow earthquakes. *Nature Communications*, *14*(1), 5101. doi: https://doi.org/10.1038/s41467-023-40762-4

Ariyoshi, K., Ampuero, J.-P., Bürgmann, R., Matsuzawa, T., Hasegawa, A., Hino, R., & Hori, T. (2019). Quantitative relationship between aseismic slip propagation speed and frictional properties. *Tectonophysics*, *767*, 128151. Retrieved from https://www.sciencedirect.com/science/article/pii/S0040195119302525 doi: https://doi.org/10.1016/j.tecto.2019.06.021

Blewitt, G., Hammond, W. C., & Kreemer, C. (2018). Harnessing the gps data explosion for interdisciplinary science. *EOS*, *99*. doi: 10.1029/2018EO104623

Choi, K., Bilich, A., Larson, K. M., & Axelrad, P. (2004). Modified sidereal filter-

ing: Implications for high-rate gps positioning. *Geophysical Research Letters*, *31*(22). doi: 10.1029/2004GL021621

DeMets, C., Gordon, R. G., & Argus, D. F. (2010, 04). Geologically current plate motions. *Geophysical Journal International*, *181*(1), 1-80. Retrieved from `https://doi.org/10.1111/j.1365-246X.2009.04491.x` doi: 10.1111/j.1365-246X.2009.04491.x

Earthquake Source Model Database. (2024). *s1968hyugax01yagi [dataset].* Retrieved from `http://equake-rc.info/SRCMOD/searchmodels/viewmodel/s1968HYUGAx01YAGI/`

Frank, W. B., Poli, P., & Perfettini, H. (2017). Mapping the rheology of the central chile subduction zone with aftershocks. *Geophysical Research Letters*, *44*(11), 5374-5382. Retrieved from `https://agupubs.onlinelibrary.wiley.com/doi/abs/10.1002/2016GL072288` doi: https://doi.org/10.1002/2016GL072288

Igarashi, T. (2020). Catalog of small repeating earthquakes for the japanese islands. *Earth, Planets and Space*, *72*(1), 1–8. doi: https://doi.org/10.1186/s40623-020-01205-2

Ioki, K., Yamashita, Y., & Kase, Y. (2023). Effects of the tsunami generated by the 1662 hyuga-nada earthquake off miyazaki prefecture, japan. *Pure and Applied Geophysics*, *180*(6), 1897–1907. doi: https://doi.org/10.1007/s00024-022-03198-3

Itoh, Y., & Aoki, Y. (2022). On the performance of position-domain sidereal filter for 30-s kinematic gps to mitigate multipath errors. *Earth, Planets and Space*, *74*(1), 1–20. doi: 10.1186/s40623-022-01584-8

Itoh, Y., Nishimura, T., Ariyoshi, K., & Matsumoto, H. (2019). Interplate slip following the 2003 tokachi-oki earthquake from ocean bottom pressure gauge and land gnss data. *Journal of Geophysical Research: Solid Earth*, *124*(4), 4205-4230. Retrieved from `https://agupubs.onlinelibrary.wiley.com/doi/abs/10.1029/2018JB016328` doi: https://doi.org/10.1029/2018JB016328

Itoh, Y., Socquet, A., & Radiguet, M. (2023). Largest aftershock nucleation driven by afterslip during the 2014 iquique sequence. *Geophysical Research Letters*, *50*(24), e2023GL104852. Retrieved from `https://agupubs.onlinelibrary.wiley.com/doi/abs/10.1029/2023GL104852` (e2023GL104852 2023GL104852) doi: https://doi.org/10.1029/2023GL104852

Iwasaki, T. (2024). *Plate boundary models in and around japan [dataset].* Retrieved from `http://evrrss.eri.u-tokyo.ac.jp/database/PLATEmodel/`

Iwasaki, T., Sato, H., Ishiyama, T., Shinohara, M., & Hashima, A. (2015, December). Fundamental structure model of island arcs and subducted plates in and around Japan. In *Agu fall meeting abstracts* (Vol. 2015, p. T31B-2878).

Japan Meteorological Agency. (2024a). *[dataset].* Retrieved from `https://www.data.jma.go.jp/svd/eqev/data/bulletin/hypo_e.html`

Japan Meteorological Agency. (2024b). *[dataset].* Retrieved from `https://www.data.jma.go.jp/eqev/data/daily_map/index.html`

Kano, M., Aso, N., Matsuzawa, T., Ide, S., Annoura, S., Arai, R., ... others (2018). Development of a slow earthquake database. *Seismological Research Letters*, *89*(4), 1566–1575. doi: https://doi.org/10.1785/0220180021

Kato, A., & Obara, K. (2014). Step-like migration of early aftershocks following the 2007 m 6.7 noto-hanto earthquake, japan. *Geophysical Research Letters*, *41*(11), 3864-3869. Retrieved from `https://agupubs.onlinelibrary.wiley.com/doi/abs/10.1002/2014GL060427` doi: https://doi.org/10.1002/2014GL060427

Kubo, H., & Nishikawa, T. (2020). Relationship of preseismic, coseismic, and postseismic fault ruptures of two large interplate aftershocks of the 2011 tohoku earthquake with slow-earthquake activity. *Scientific reports*, *10*(1), 12044. doi: https://doi.org/10.1038/s41598-020-68692-x

Lindquist, K. G., Engle, K., Stahlke, D., & Price, E. (2004). Global topography and bathymetry grid improves research efforts. *Eos, Transactions American Geophysical Union*, *85*(19), 186-186. Retrieved from `https://agupubs.onlinelibrary.wiley.com/doi/abs/10.1029/2004EO190003` doi: https://doi.org/10.1029/2004EO190003

Mai, P. M., & Thingbaijam, K. K. S. (2014, 10). SRCMOD: An Online Database of Finite-Fault Rupture Models. *Seismological Research Letters*, *85*(6), 1348-1357. Retrieved from `https://doi.org/10.1785/0220140077` doi: 10.1785/0220140077

Marone, C. J., Scholtz, C. H., & Bilham, R. (1991). On the mechanics of earthquake afterslip. *Journal of Geophysical Research: Solid Earth*, *96*(B5), 8441-8452. Retrieved from `https://agupubs.onlinelibrary.wiley.com/doi/abs/10.1029/91JB00275` doi: https://doi.org/10.1029/91JB00275

Miyazaki, S., Segall, P., Fukuda, J., & Kato, T. (2004). Space time distribution of afterslip following the 2003 tokachi-oki earthquake: Implications for variations in fault zone frictional properties. *Geophysical Research Letters*, *31*(6). Retrieved from `https://agupubs.onlinelibrary.wiley.com/doi/abs/10.1029/2003GL019410` doi: https://doi.org/10.1029/2003GL019410

Mochizuki, K., Yamada, T., Shinohara, M., Yamanaka, Y., & Kanazawa, T. (2008). Weak interplate coupling by seamounts and repeating ¡i¿m¡/i¿ 7 earthquakes. *Science*, *321*(5893), 1194-1197. Retrieved from `https://www.science.org/doi/abs/10.1126/science.1160250` doi: 10.1126/science.1160250

Nevada Geodetic Laboratory. (2024). *[dataset]*. Retrieved from `http://geodesy.unr.edu/`

Nishikawa, T., Matsuzawa, T., Ohta, K., Uchida, N., Nishimura, T., & Ide, S. (2019). The slow earthquake spectrum in the japan trench illuminated by the s-net seafloor observatories. *Science*, *365*(6455), 808-813. Retrieved from `https://www.science.org/doi/abs/10.1126/science.aax5618` doi: 10.1126/science.aax5618

Nishimura, S., & Hashimoto, M. (2006). A model with rigid rotations and slip deficits for the gps-derived velocity field in southwest japan. *Tectonophysics*, *421*(3), 187-207. Retrieved from `https://www.sciencedirect.com/science/article/pii/S0040195106002368` doi: https://doi.org/10.1016/j.tecto.2006.04.017

Nishimura, T., Yokota, Y., Tadokoro, K., & Ochi, T. (2018, 02). Strain partitioning and interplate coupling along the northern margin of the Philippine Sea plate, estimated from Global Navigation Satellite System and Global Positioning System-Acoustic data. *Geosphere*, *14*(2), 535-551. Retrieved from `https://doi.org/10.1130/GES01529.1` doi: 10.1130/GES01529.1

Noda, A., Saito, T., & Fukuyama, E. (2018). Slip-deficit rate distribution along the nankai trough, southwest japan, with elastic lithosphere and viscoelastic asthenosphere. *Journal of Geophysical Research: Solid Earth*, *123*(9), 8125-8142. Retrieved from `https://agupubs.onlinelibrary.wiley.com/doi/abs/10.1029/2018JB015515` doi: https://doi.org/10.1029/2018JB015515

Okada, Y. (1985, 08). Surface deformation due to shear and tensile faults in a half-space. *Bulletin of the Seismological Society of America*, *75*(4), 1135-1154. Retrieved from `https://doi.org/10.1785/BSSA0750041135` doi: 10.1785/BSSA0750041135

Okada, Y., Nishimura, T., Tabei, T., Matsushima, T., & Hirose, H. (2022). Development of a detection method for short-term slow slip events using gnss data and its application to the nankai subduction zone. *Earth, Planets and Space*, *74*(1), 1–18.

Okazaki, T., Fukahata, Y., & Nishimura, T. (2021). Consistent estimation of strain-rate fields from gnss velocity data using basis function expansion with abic. *Earth, Planets and Space*, *73*, 1–22. doi: https://doi.org/10.1186/

423 s40623-021-01474-5

424 Okino, K. (2015). Magnetic anomalies in the philippine sea: Implications for re-
425 gional tectonics. *Journal of Geography (Chigaku Zasshi)*, *124*(5), 729-747. doi:
426 10.5026/jgeography.124.729

427 Ozawa, S., Muneakane, H., & Suito, H. (2024). Time-dependent model-
428 ing of slow-slip events along the nankai trough subduction zone, japan,
429 within the 2018–2023 period. *Earth, Planets and Space*, *76*(1), 23. doi:
430 https://doi.org/10.1186/s40623-024-01970-4

431 Peng, Z., & Zhao, P. (2009). Migration of early aftershocks following the 2004 park-
432 field earthquake. *Nature Geoscience*, *2*(12), 877–881. doi: https://doi.org/10
433 .1038/ngeo697

434 Perfettini, H., & Avouac, J.-P. (2004). Postseismic relaxation driven by brittle
435 creep: A possible mechanism to reconcile geodetic measurements and the de-
436 cay rate of aftershocks, application to the chi-chi earthquake, taiwan. *Journal*
437 *of Geophysical Research: Solid Earth*, *109*(B2). Retrieved from `https://`
438 `agupubs.onlinelibrary.wiley.com/doi/abs/10.1029/2003JB002488` doi:
439 https://doi.org/10.1029/2003JB002488

440 Perfettini, H., Avouac, J.-P., Tavera, H., Kositsky, A., Nocquet, J.-M., Bondoux, F.,
441 . . . others (2010). Seismic and aseismic slip on the central peru megathrust.
442 *Nature*, *465*(7294), 78–81. doi: https://doi.org/10.1038/nature09062

443 Perfettini, H., Frank, W. B., Marsan, D., & Bouchon, M. (2018). A model of after-
444 shock migration driven by afterslip. *Geophysical Research Letters*, *45*(5), 2283-
445 2293. Retrieved from `https://agupubs.onlinelibrary.wiley.com/doi/abs/`
446 `10.1002/2017GL076287` doi: https://doi.org/10.1002/2017GL076287

447 Ragheb, A., Clarke, P. J., & Edwards, S. (2007). Gps sidereal filtering: coordinate-
448 and carrier-phase-level strategies. *Journal of Geodesy*, *81*(5), 325–335. doi: 10
449 .1007/s00190-006-0113-1

450 Rolandone, F., Nocquet, J.-M., Mothes, P. A., Jarrin, P., Vallée, M., Cubas, N., . . .
451 Font, Y. (2018). Areas prone to slow slip events impede earthquake rupture
452 propagation and promote afterslip. *Science Advances*, *4*(1), eaao6596. Re-
453 trieved from `https://www.science.org/doi/abs/10.1126/sciadv.aao6596`
454 doi: 10.1126/sciadv.aao6596

455 Ross, Z. E., Rollins, C., Cochran, E. S., Hauksson, E., Avouac, J.-P., & Ben-Zion, Y.
456 (2017). Aftershocks driven by afterslip and fluid pressure sweeping through
457 a fault-fracture mesh. *Geophysical Research Letters*, *44*(16), 8260-8267.
458 Retrieved from `https://agupubs.onlinelibrary.wiley.com/doi/abs/`
459 `10.1002/2017GL074634` doi: https://doi.org/10.1002/2017GL074634

460 Ruh, J. B., Sallarès, V., Ranero, C. R., & Gerya, T. (2016). Crustal deforma-
461 tion dynamics and stress evolution during seamount subduction: High-
462 resolution 3-d numerical modeling. *Journal of Geophysical Research: Solid*
463 *Earth*, *121*(9), 6880-6902. Retrieved from `https://agupubs.onlinelibrary`
464 `.wiley.com/doi/abs/10.1002/2016JB013250` doi: https://doi.org/10.1002/
465 2016JB013250

466 Sagiya, T. (2004). A decade of geonet: 1994-2003. *Earth, Planets and Space*, *56*(8),
467 xxix-xli. doi: 10.1186/BF03353077

468 Sagiya, T., Miyazaki, S., & Tada, T. (2000). Continuous gps array and present-day
469 crustal deformation of japan. *Pure and applied Geophysics*, *157*, 2303–2322.
470 doi: https://doi.org/10.1007/PL00022507

471 Sagiya, T., & Thatcher, W. (1999). Coseismic slip resolution along a plate bound-
472 ary megathrust: The nankai trough, southwest japan. *Journal of Geophysical*
473 *Research: Solid Earth*, *104*(B1), 1111-1129. Retrieved from `https://agupubs`
474 `.onlinelibrary.wiley.com/doi/abs/10.1029/98JB02644` doi: https://doi
475 .org/10.1029/98JB02644

476 Savage, J. C. (1983). A dislocation model of strain accumulation and release at a
477 subduction zone. *Journal of Geophysical Research: Solid Earth*, *88*(B6), 4984-

4996. Retrieved from `https://agupubs.onlinelibrary.wiley.com/doi/abs/` `10.1029/JB088iB06p04984` doi: https://doi.org/10.1029/JB088iB06p04984

Scholz, C. H. (1998). Earthquakes and friction laws. *Nature*, *391*(6662), 37–42. doi: https://doi.org/10.1038/34097

Science of Slow Earthquakes. (2024). *Slow earthquake database [dataset].* Retrieved from `http://www-solid.eps.s.u-tokyo.ac.jp/~sloweq/`

Smith, W. H. F., & Sandwell, D. T. (1997). Global sea floor topography from satellite altimetry and ship depth soundings. *Science*, *277*(5334), 1956-1962. Retrieved from `https://www.science.org/doi/abs/10.1126/` `science.277.5334.1956` doi: 10.1126/science.277.5334.1956

Sun, T., Saffer, D., & Ellis, S. (2020). Mechanical and hydrological effects of seamount subduction on megathrust stress and slip. *Nature Geoscience*, *13*(3), 249–255. doi: https://doi.org/10.1038/s41561-020-0542-0

Takagi, R., Obara, K., & Maeda, T. (2016). Slow slip event within a gap between tremor and locked zones in the nankai subduction zone. *Geophysical Research Letters*, *43*(3), 1066-1074. Retrieved from `https://agupubs.onlinelibrary` `.wiley.com/doi/abs/10.1002/2015GL066987` doi: https://doi.org/10.1002/ 2015GL066987

Takagi, R., Uchida, N., & Obara, K. (2019). Along-strike variation and migration of long-term slow slip events in the western nankai subduction zone, japan. *Journal of Geophysical Research: Solid Earth*, *124*(4), 3853-3880. Retrieved from `https://agupubs.onlinelibrary.wiley.com/doi/abs/` `10.1029/2018JB016738` doi: https://doi.org/10.1029/2018JB016738

Takemura, S., Okuwaki, R., Kubota, T., Shiomi, K., Kimura, T., & Noda, A. (2020a, February). *3D CMT catalogue of moderate size offshore earthquakes along the Nankai Trough.* Zenodo. Retrieved from `https://doi.org/10.5281/` `zenodo.3674161` doi: 10.5281/zenodo.3674161

Takemura, S., Okuwaki, R., Kubota, T., Shiomi, K., Kimura, T., & Noda, A. (2020b, 05). Centroid moment tensor inversions of offshore earthquakes using a three-dimensional velocity structure model: slip distributions on the plate boundary along the Nankai Trough. *Geophysical Journal International*, *222*(2), 1109-1125. Retrieved from `https://doi.org/10.1093/gji/ggaa238` doi: 10.1093/gji/ggaa238

Twardzik, C., Vergnolle, M., Sladen, A., & Avallone, A. (2019). Unravelling the contribution of early postseismic deformation using sub-daily gnss positioning. *Scientific reports*, *9*(1), 1775. doi: https://doi.org/10.1038/ s41598-019-39038-z

Uchida, N., Takagi, R., Asano, Y., & Obara, K. (2020). Migration of shallow and deep slow earthquakes toward the locked segment of the nankai megathrust. *Earth and Planetary Science Letters*, *531*, 115986. Retrieved from `https://` `www.sciencedirect.com/science/article/pii/S0012821X19306788` doi: https://doi.org/10.1016/j.epsl.2019.115986

Wallace, L. M., Ellis, S., Miyao, K., Miura, S., Beavan, J., & Goto, J. (2009, 02). Enigmatic, highly active left-lateral shear zone in southwest Japan explained by aseismic ridge collision. *Geology*, *37*(2), 143-146. Retrieved from `https://doi.org/10.1130/G25221A.1` doi: 10.1130/G25221A.1

Wallace, L. M., Hreinsdóttir, S., Ellis, S., Hamling, I., D'Anastasio, E., & Denys, P. (2018). Triggered slow slip and afterslip on the southern hikurangi subduction zone following the kaikōura earthquake. *Geophysical Research Letters*, *45*(10), 4710-4718. Retrieved from `https://agupubs.onlinelibrary` `.wiley.com/doi/abs/10.1002/2018GL077385` doi: https://doi.org/10.1002/ 2018GL077385

Wang, K., & Bilek, S. L. (2011, 09). Do subducting seamounts generate or stop large earthquakes? *Geology*, *39*(9), 819-822. Retrieved from `https://doi.org/10` `.1130/G31856.1` doi: 10.1130/G31856.1

Wang, K., & Bilek, S. L.   (2014).   Invited review paper: Fault creep caused by subduction of rough seafloor relief.   *Tectonophysics*, *610*, 1-24.   Retrieved from `https://www.sciencedirect.com/science/article/pii/S0040195113006896` doi: https://doi.org/10.1016/j.tecto.2013.11.024

Wang, L., Wang, R., Roth, F., Enescu, B., Hainzl, S., & Ergintav, S.   (2009, 09). Afterslip and viscoelastic relaxation following the 1999 M 7.4 İzmit earthquake from GPS measurements.   *Geophysical Journal International*, *178*(3), 1220-1237. Retrieved from `https://doi.org/10.1111/j.1365-246X.2009.04228.x` doi: 10.1111/j.1365-246X.2009.04228.x

Wang, R., Diao, F., & Hoechner, A. (2013a). Sdm-a geodetic inversion code incorporating with layered crust structure and curved fault geometry.   In *Egu general assembly conference abstracts* (pp. EGU2013–2411).

Wang, R., Diao, F., & Hoechner, A.   (2013b).   Sdm – a geodetic inversion code incorporating with layered crust structure and curved fault geometry. *GFZ [Software]*.   Retrieved from `https://www.gfz-potsdam.de/pub/home/turk/wang/` doi: https://gfzpublic.gfz-potsdam.de/pubman/item/item_1975902

Wdowinski, S., Bock, Y., Zhang, J., Fang, P., & Genrich, J.   (1997).   Southern california permanent gps geodetic array: Spatial filtering of daily positions for estimating coseismic and postseismic displacements induced by the 1992 landers earthquake.   *Journal of Geophysical Research: Solid Earth*, *102*(B8), 18057-18070. doi: 10.1029/97JB01378

Yagi, Y., Kikuchi, M., & Sagiya, T.   (2001).   Co-seismic slip, post-seismic slip, and aftershocks associated with two large earthquakes in 1996 in hyuga-nada, japan. *Earth, planets and space*, *53*(8), 793–803. doi: https://doi.org/10.1186/BF03351677

Yagi, Y., Kikuchi, M., Yoshida, S., & Sagiya, T.   (1999).   Comparison of the coseismic rupture with the aftershock distribution in the hyuga-nada earthquakes of 1996.   *Geophysical Research Letters*, *26*(20), 3161-3164.   Retrieved from `https://agupubs.onlinelibrary.wiley.com/doi/abs/10.1029/1999GL005340` doi: https://doi.org/10.1029/1999GL005340

Yagi, Y., Kikuchi, M., Yoshida, S., & Yamanaka, Y.   (1998).   Source process of the hyuga-nada earthquake of april 1, 1968 (m_{JMA}7.5), and its relationship to the subsequent seismicity.   *Zisin (Journal of the Seismological Society of Japan. 2nd ser.)*, *51*(1), 139-148. doi: 10.4294/zisin1948.51.1_139

Yamamoto, Y., Obana, K., Takahashi, T., Nakanishi, A., Kodaira, S., & Kaneda, Y.   (2013).   Imaging of the subducted kyushu-palau ridge in the hyuga-nada region, western nankai trough subduction zone.   *Tectonophysics*, *589*, 90-102. Retrieved from `https://www.sciencedirect.com/science/article/pii/S0040195113000103` doi: https://doi.org/10.1016/j.tecto.2012.12.028

Yamashita, Y., Shimizu, H., & Goto, K.   (2012).   Small repeating earthquake activity, interplate quasi-static slip, and interplate coupling in the hyuga-nada, southwestern japan subduction zone.   *Geophysical Research Letters*, *39*(8). Retrieved from `https://agupubs.onlinelibrary.wiley.com/doi/abs/10.1029/2012GL051476` doi: https://doi.org/10.1029/2012GL051476

Yamashita, Y., Shinohara, M., & Yamada, T.   (2021).   Shallow tectonic tremor activities in hyuga-nada, nankai subduction zone, based on long-term broadband ocean bottom seismic observations.   *Earth, Planets and Space*, *73*, 1–11.   doi: https://doi.org/10.1186/s40623-021-01533-x

Yamashita, Y., Yakiwara, H., Asano, Y., Shimizu, H., Uchida, K., Hirano, S., . . . Obara, K.   (2015).   Migrating tremor off southern kyushu as evidence for slow slip of a shallow subduction interface.   *Science*, *348*(6235), 676-679. Retrieved from `https://www.science.org/doi/abs/10.1126/science.aaa4242`   doi: 10.1126/science.aaa4242
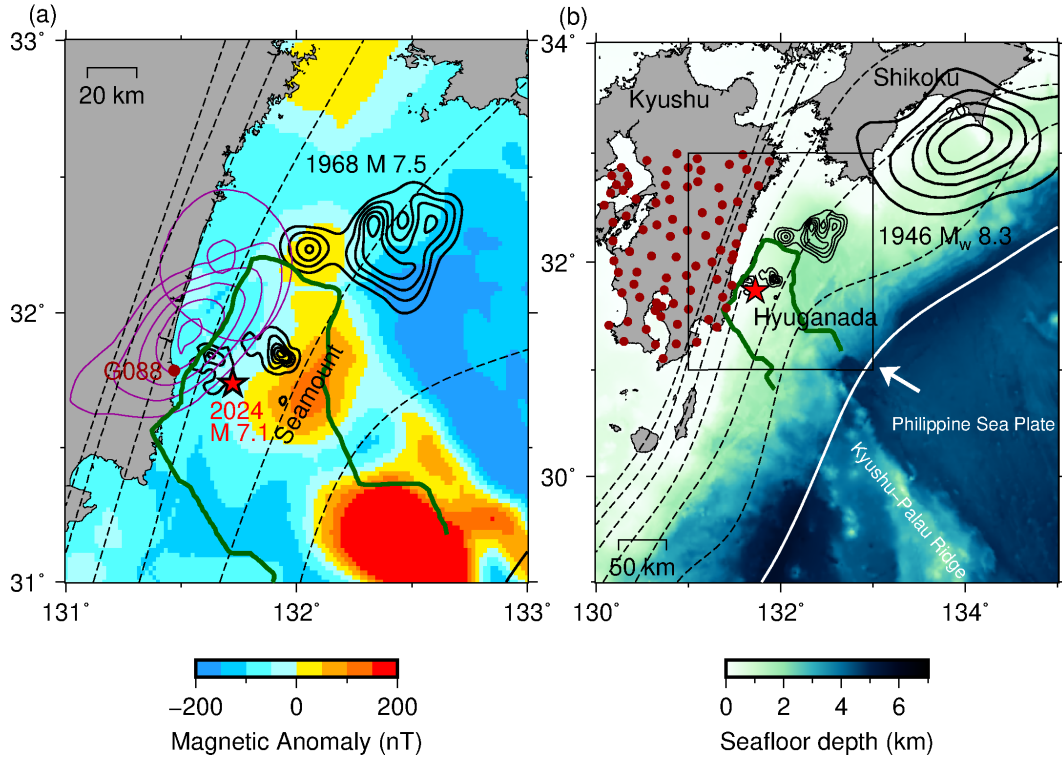
Figure 1. Tectonic setting. (a) The red star indicates the epicenter of the 2024 Hyuganada earthquake determined by Japan Meteorological Agency. The black solid contours indicate the 1968 (every 0.6 m from 1.2 m) and the two 1996 (every 0.5 m from 0.5 m for both, near the 2024 epicenter) Hyuganada earthquakes (Yagi et al., 1998, 1999). Two afterslip models following the two 1996 earthquake are drown in purple (every 2 cm from 4 cm Yagi et al., 2001). The broken contours indicate slab surface depth at an interval of 10 km from 10 km (Iwasaki et al., 2015). The background color in the sea area is RTP magnetic anomaly (Arai et al., 2023; Okino, 2015). The dark green curve indicates the estimate of spatial range of the subducted KPR inferred from a low seismic velocity belt (Yamamoto et al., 2013). The brown dot indicates the location of an example GNSS site, G088, shown in Figure 2. (b) Broader map. Brown dots indicate all the GNSS sites used to infer the slip distributions. The rupture area 1946 M_w8.3 Nankaido earthquake is contoured at an interval of 2 m from 2 m (Sagiya & Thatcher, 1999). The vector seaward of the trench is a motion direction of the Philippine Sea Plate motion with respect to the Amur plate (DeMets et al., 2010). The seafloor depth in background is taken from Smith and Sandwell (1997).
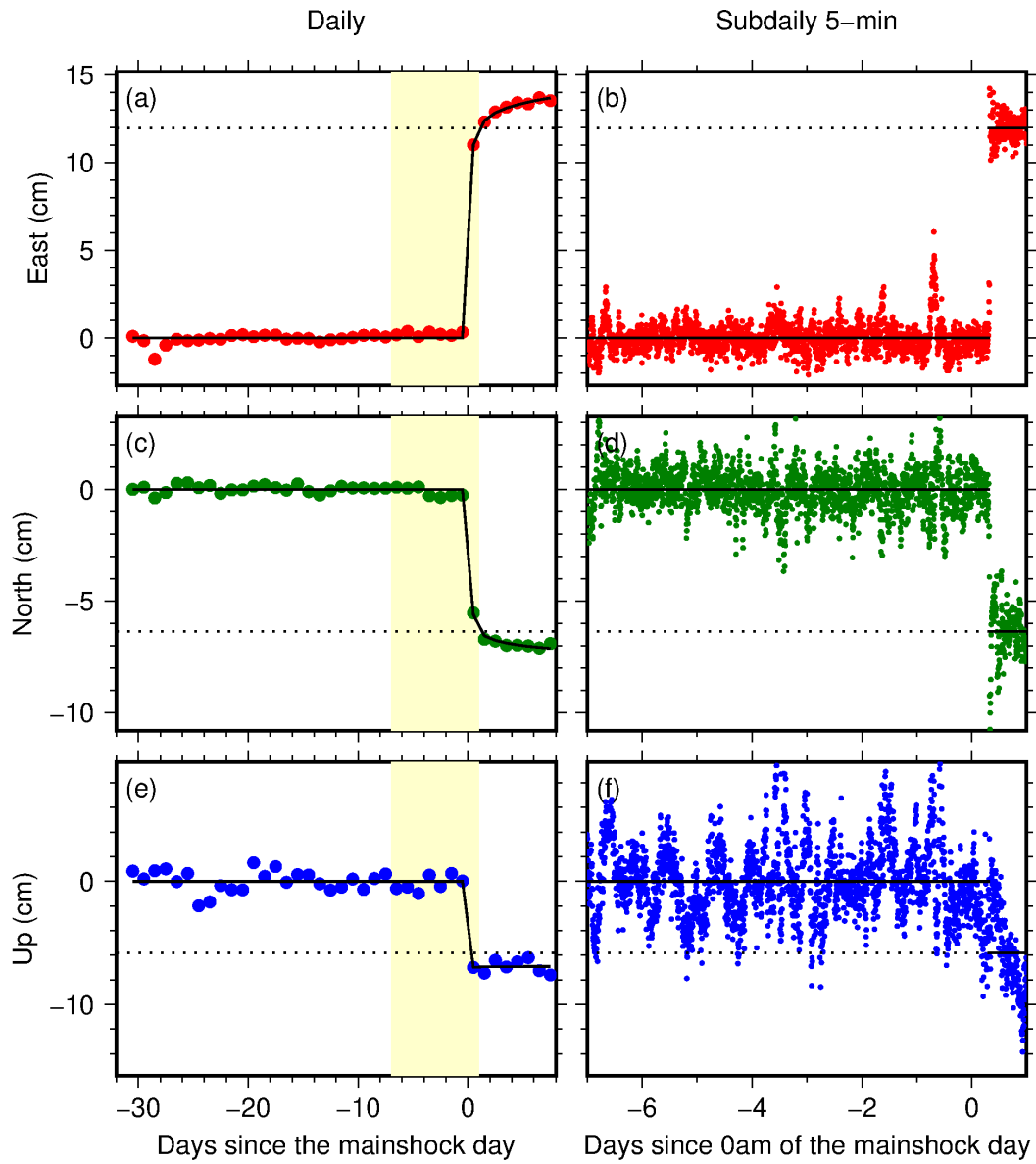
Figure 2. An example of GNSS time series at site G088 (Figure 1a). (a) East component of daily time series (red) with a function fit to it (black) using Equation (1). The dotted line is an immediate post-mainshock position inferred from 5-minute coordinates in (b). (b) East component of 5-minute time series (red) with the averaged pre- and post-mainshock positions (black). (c-f) Same as (a-b) but for north (c-d) and vertical (e-f) components.
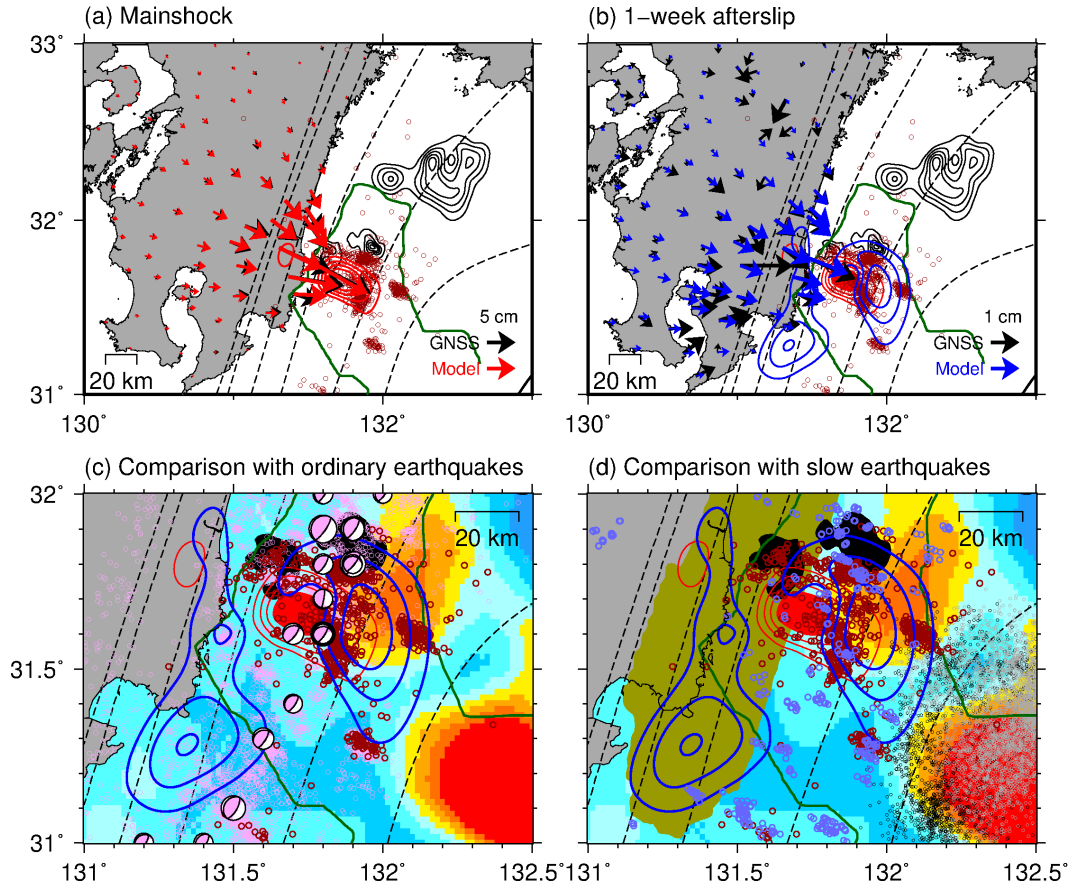
Figure 3. Inversion results. (a-b) Contours indicate the estimated coseismic (a, every 50 cm from 50 cm, red) and 1-week afterslip (b every 5 cm from 5 cm, blue). The vectors indicate horizontal co- (a) and 1-week post-seismic (b) displacements (black) with model predictions from the coseismic slip (a, red) and afterslip (b, blue). Vertical displacements are shown in Figure S1. The brown open dots indicate 1-week aftershocks reported by JMA. (c-d) Comparison of the estimated coseismic slip and afterslip with various tectonic slip phenomena. (c) The pink open dots indicate ordinary seismicity from April 1, 2016, to August 7, 2024, as reported by JMA. The beachballs indicate Centroid Moment Tensor (CMT) solutions of moderate earthquakes ranging between M_w 4.1 and 5.5 from 2004 to 2019 (Takemura et al., 2020b). (d) Blue open dots indicate repeating earthquakes from 1982 to 2019 (Igarashi, 2020). The area with more than 5 short-term SSEs from 1997 to 2020 is drawn in olive (Okada et al., 2022). The black and grey open dots tectonic tremors in 2013 and 2014-2017, respectively (Yamashita et al., 2015, 2021). Refer to Figure 1 for other elements.
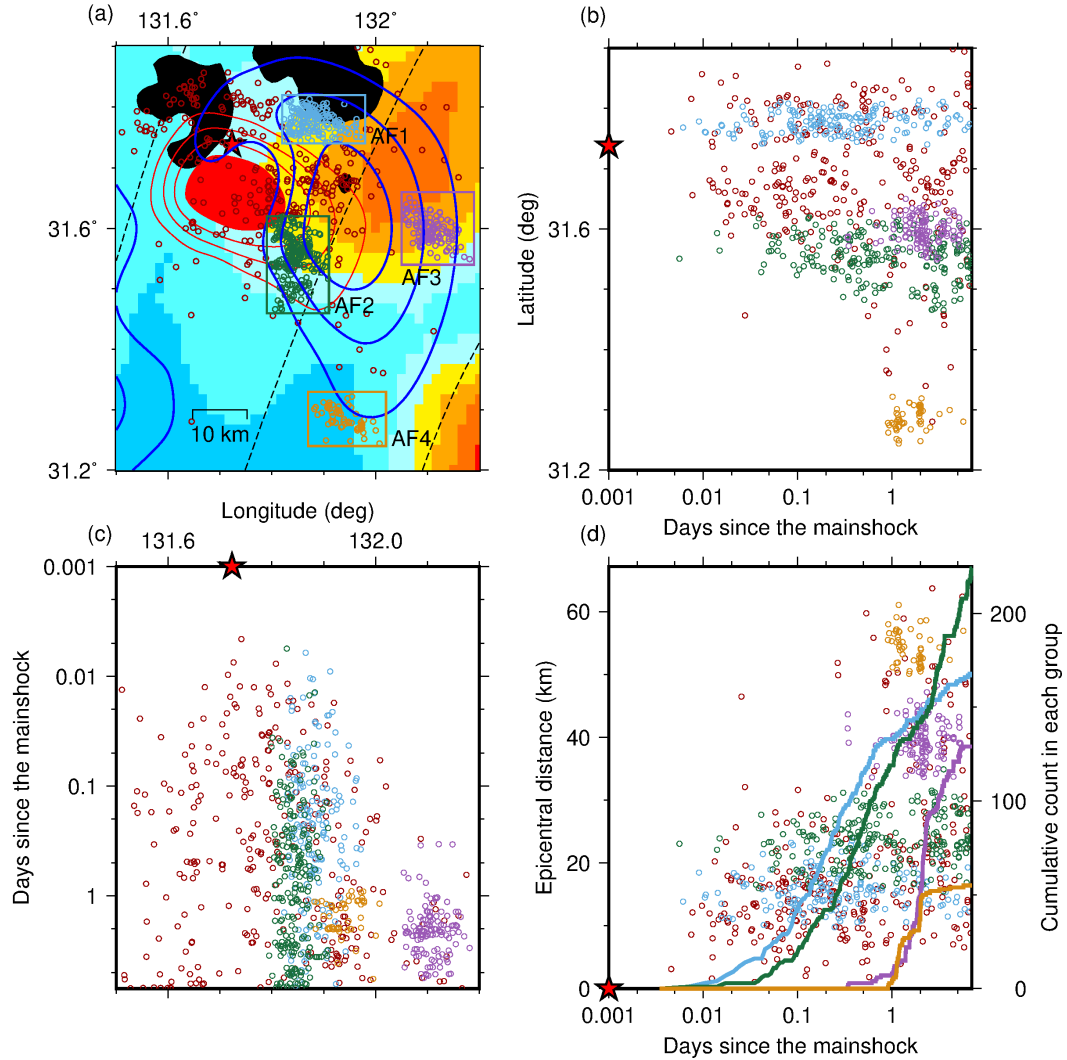
Figure 4. Seismicity analysis results. (a) Zoom in plot of the coseismic slip and afterslip area. The two 1968 rupture areas are drawn in black. The selected four aftershock clusters are drawn with different colors as labeled. (b) Temporal evolution of seismicity in the latitude direction. The star indicates the mainshock latitude. Refer to (a) for different colors. (c) Same as (b) but in the longitude direction. (d) Same as (b-c) but with respect to the epicentral distance. The curves indicate cumulative event counts measured every 5 minutes in each cluster with the corresponding colors. Refer to Figure 1 for other elements.
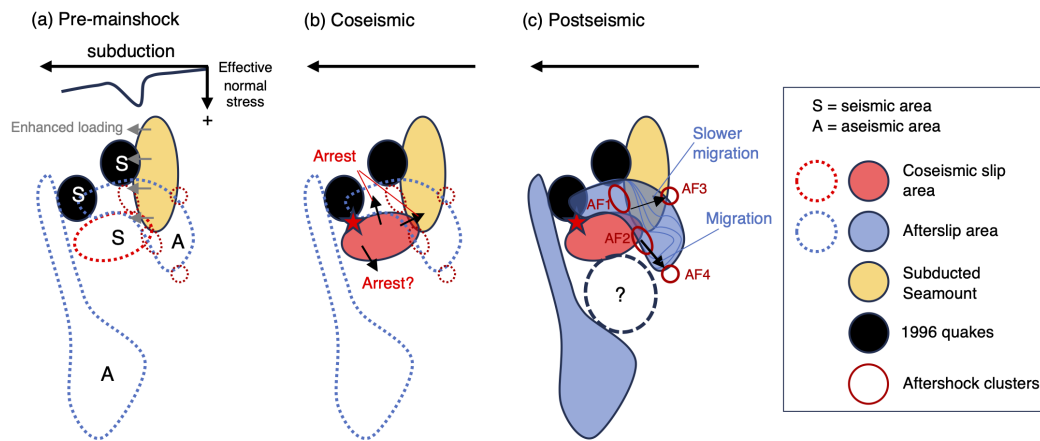
Figure 5. Schetch of the proposed occurrence scenario of the 2024 Hyuganada mainshock and afterslip. The blue curves in the afterslip patch in (c) indicate the temporal evolution of slip front we inferred from the temporal evolution of aftershock activities (Figure 4d).

Supporting Information for "Coseimsic slip and afterslip of the 2024 Hyuganada earthquake modulated by subducted seamount"

Yuji Itoh[1]

[1]Earthquake Research Institute, The University of Tokyo, Japan

Contents of this file
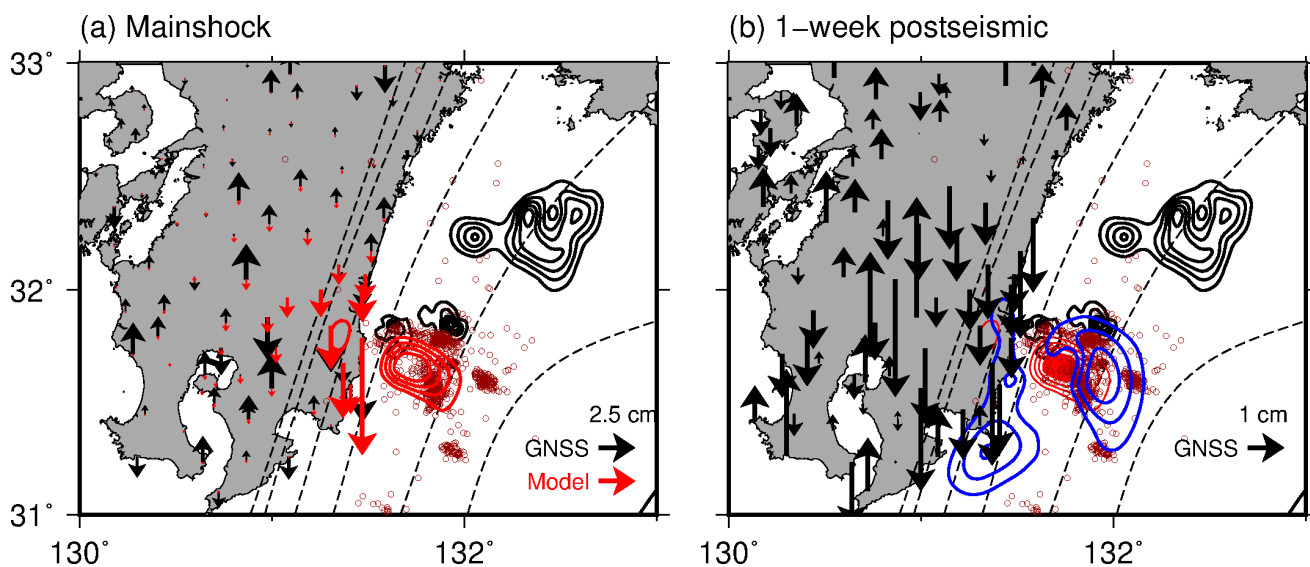
1. Figures S1 to S4

———

October 2, 2024, 1:51am

Figure S1. Coseismic (a) and 1-week postseismic (b) displacements. Refer to Figure 3 for other elements. No postseismic model displacements are drawn because we did not invert the vertical postseismic displacements. Refer to Figure 3 for other elements.
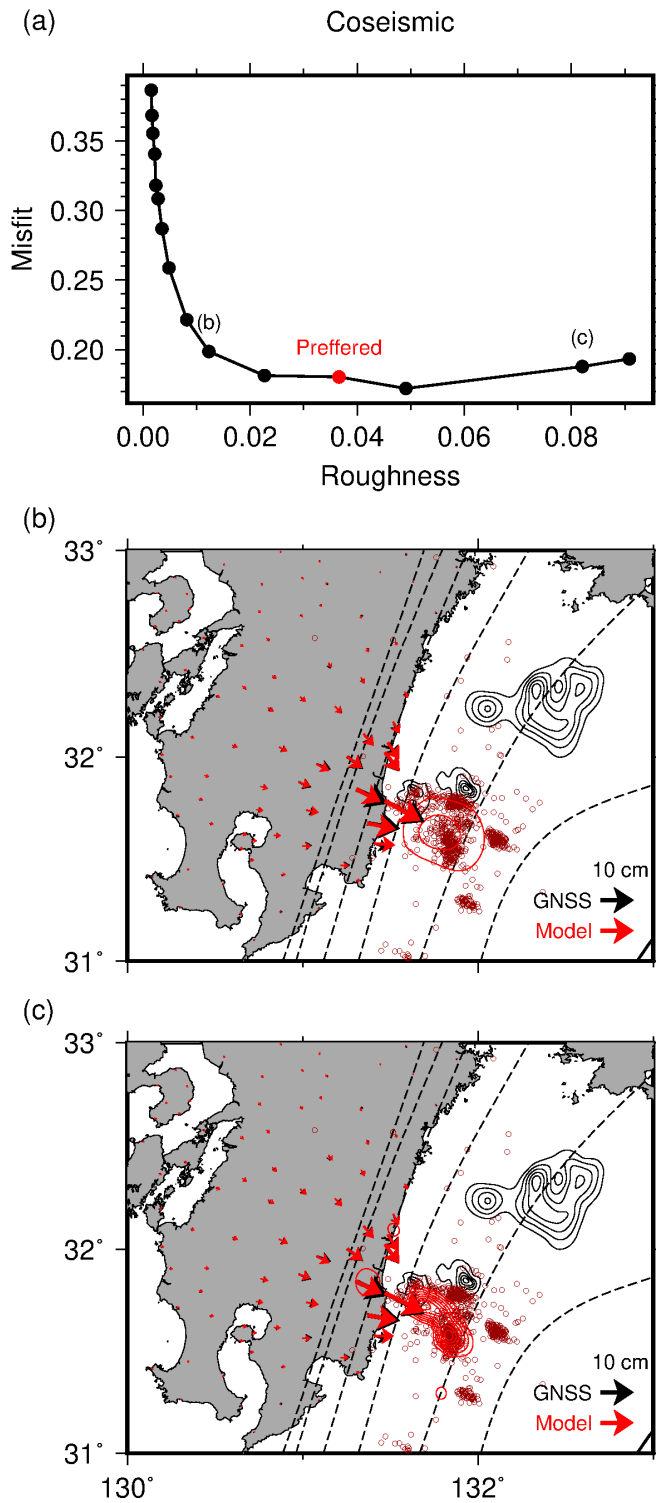
Figure S2. (a) Trade-off curve of the slip roughness and misfit for the coseismic slip. The red dot indicates the preferred solution in Figure 3a. (b-c) Examples of smoother (b) and rougher (c) solutions. Refer to Figure 3 for other elements.
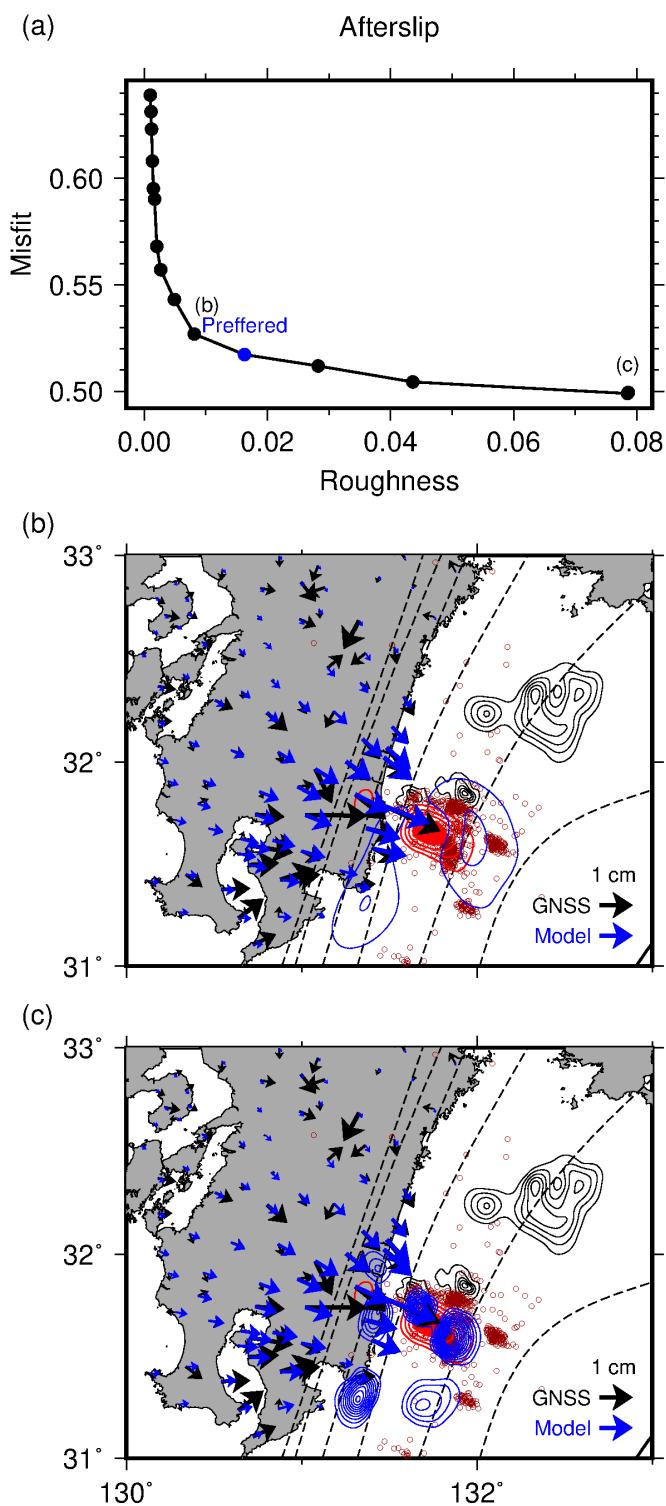
Figure S3. (a) Trade-off curve of the slip roughness and misfit for the 1-week afterslip. The blue dot indicates the preferred solution in Figure 3b. (b-c) Examples of smoother (b) and rougher (c) solutions. Refer to Figure 3 for other elements.
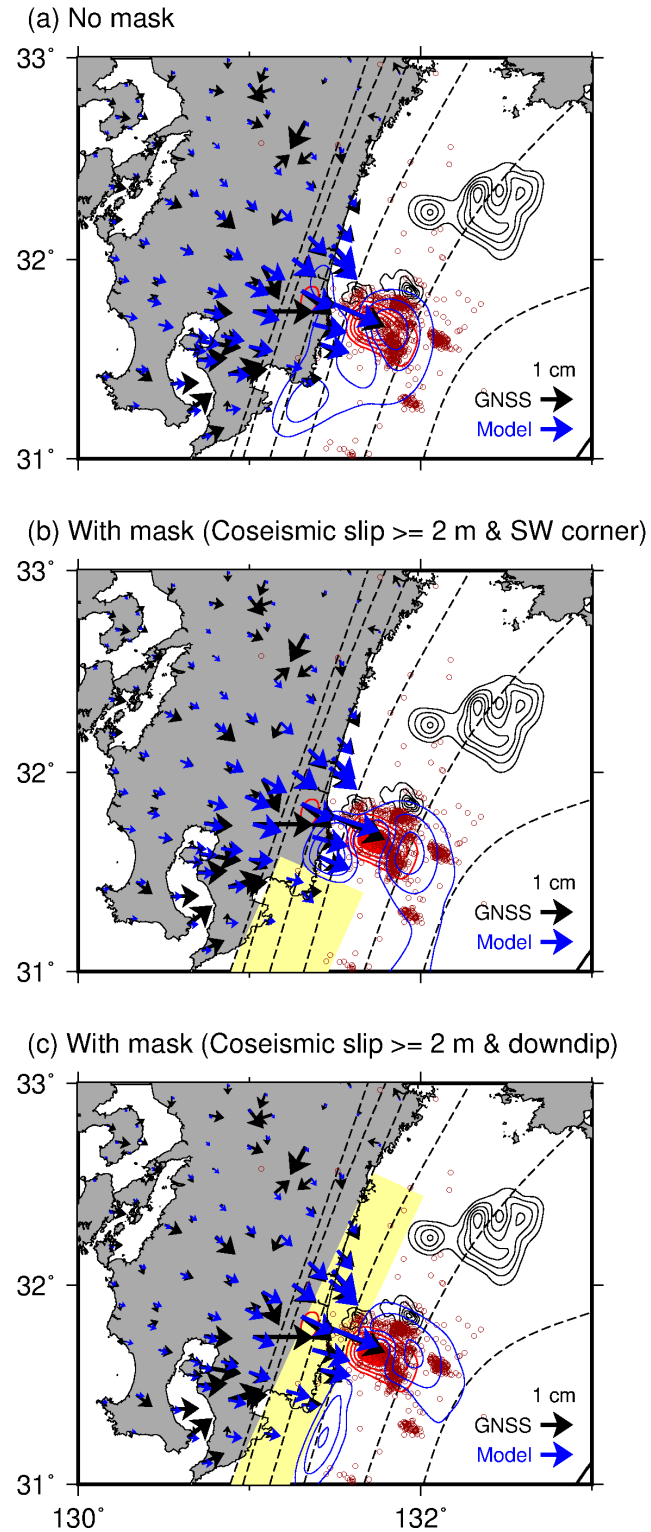
Figure S4.   (a) The estimated 1-week afterslip distribution without any mask of slip area. (b-c) Same as (a) but slip in the area of the coseismic slip more than 2 m (filled in red) and the area highlighted in yellow is constrained to be zero. Refer to Figure 3 for other elements.